A Liquid-Metal-Enabled Reconfigurable Feed Network for Multi-Polarization Arrays

Yi-Wen Wu, *Member, IEEE*, James Kelly, *Member, IEEE*, Lu Qian, *Member, IEEE*, Costas Constantinou, *Senior Member, IEEE*, Farhad Ghorbani, Jiafeng Zhou, *Senior Member, IEEE*, Yi Huang, *Fellow, IEEE*, and Yi Wang, *Senior Member, IEEE*

***Abstract*—This paper presents a novel reconfigurable feed network that allows the switch of antenna arrays across four different polarization states. Different from most previous multi-polarization antennas, the reconfiguration is implemented solely in the feed network without disturbing the radiation element. The key enabler is a reconfigurable coupler that switches between two circuit functions - a branch-line coupler or a crossover - through altering the line widths of its parallel branches. This is only made possible by using liquid metals (LMs). A double-pole-double-throw (DPDT) switch, also enabled by LM, is employed to select the input port of the reconfigurable coupler. The switch and the reconfigurable coupler form the reconfigurable feed network, providing four states of excitation to the antenna. The reconfigurable coupler, the switch and a 2×2 array have been designed and experimentally verified with the LM actuation. As a branch-line coupler, the reconfigurable coupler shows excellent amplitude and phase balance within 0.04 dB ($||S_{21}|-|S_{31}|| < 0.04$dB) and 90º at 3.5 GHz, whereas, as the crossover, it has an isolation over 25 dB. The switch exhibits an isolation of 50 dB. The measured peak gain of the array is 14.7 dBic. At 3.5 GHz, the measured axial ratio (AR) associated with the right-hand circular polarization state is 1.0 dB. The speed of switching and power handling associated with the LM have been discussed. The use of the LM has enabled a unique way of circuit reconfiguration and a full polarization-reconfigurable multi-functional antenna.**

***Index Terms*— Crossover, double-pole-double-throw switch, liquid metal, multi-polarization antenna, reconfigurable coupler.**

I. Introduction

POLARIZATION reconfigurable antennas (PRAs) have drawn great attention due to their flexibility and versatility in modern complex wireless communication systems [1]. One of the primary benefits of a PRA is its capacity to operate in environments with varying degrees of interference, since it can be switched to the polarization that provides the best signal reception [2]. They are also an excellent choice for multi-polarization applications in satellite systems and military communications.

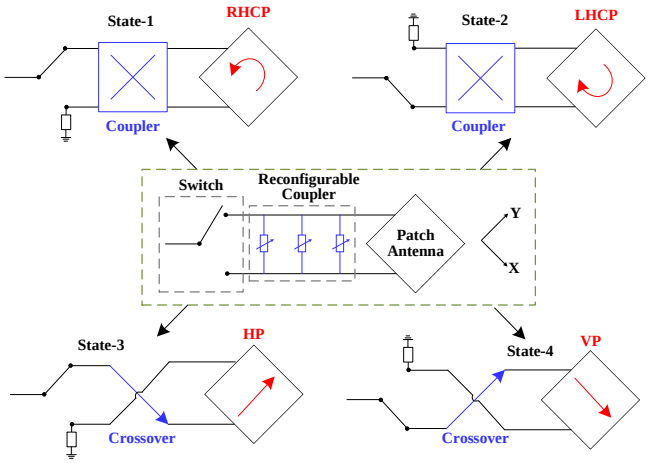

Fig. 1. Scheme of the proposed reconfigurable feed network based on a reconfigurable coupler and a switch, both enabled by liquid metals, for multi-polarization antennas.

Typically, antennas are reconfigured using radio frequency (RF) switches or tuning elements, such as PIN diodes [3], [4], [5], [6], [7], [8], [9], [10], varactor diodes [11], [12], [13], microelectromechanical systems (MEMS) switches [14], [15], and mechanical switches [16]. Circular patches are often used to design multi-polarized antennas [3], [4], [5], [7]. In [3], a C-shaped slot is introduced in a circular patch. Two PIN diodes are employed to alter the polarization state between dual linear polarizations (LP) or dual circular polarizations (CP). A ring patch antenna with two PIN diodes has three polarizations, e.g., one LP, left-hand circular polarization (LHCP) and right-hand circular polarization (RHCP) [5]. In [6], two CP modes are generated by switching on and off two PINs located in the slots of a E-shaped patch. In [7], four PIN diodes are integrated on the coplanar waveguide (CPW) transmission line with four inclined slots, which provide reconfigurable CP excitation for a circular patch antenna. Cross-bowtie radiators [8], [9] and magneto-electric dipole radiators [10] have been rotated to

Manuscript received Month DD, YYYY; revised Month DD, YYYY; accepted Month DD, YYYY.

This work was supported by UK Engineering and Physical Sciences Research Council grants EP/V008382/1. (Corresponding author: Yi-Wen Wu)

Y. Wu, Y. Wang, C. Constantinou and L. Qian are with School of Engineering, University of Birmingham, B15 2TT, United Kingdom (e-mail: y.wu.7@bham.ac.uk, y.wang.1@bham.ac.uk, c.constantinou@bham.ac.uk, l.qian.1@bham.ac.uk)

J. Kelly is with the School of Electronic Engineering and Computer Science, Queen Mary University of London, London (email: j.kelly@qmul.ac.uk)

F. Ghorbani, J. Zhou, and Y. Huang are with the Department of Electrical Engineering and Electronics, University of Liverpool, L69 3BX Liverpool, U.K. (e-mail: F.Ghorbani@liverpool.ac.uk, jiafeng.zhou@liverpool.ac.uk, yi.huang@liv.ac.uk).

generate different polarized modes. Alternatively, the different phases, needed to reconfigure the polarization of an antenna, can be obtained by tuning the capacitance of varactor diodes [11], [12], [13]. PIN diodes may be replaced by MEMS switches. For example, MEMS switches in [14] are used in the slots of E-shaped patches to generate LHCP and RHCP modes. In [15], the polarizations are obtained by using a coupler, a single-pole four-throw switch, and two single-pole double-throw switches. In [16], a reconfigurable waveguide antenna can switch between LHCP and RHCP modes through metallic posts that selectively obstruct or permit signal paths connecting the input ports to a septum-orthomode polarizer. Despite their demonstrated capability, the use of PIN diodes, varactors, and MEMS switches generally increases the circuit complexity and the insertion losses. Furthermore, the use of non-linear elements degrades communication efficiency, and the use of active components limits the power handling capability.

Liquid metal (LM) is a relatively new approach to antenna switching or reconfiguration. Unlike conventional reconfiguration mechanisms, LM-based techniques avoid the use of nonlinear elements and enhance power capacity [17], [18]. Moreover, the intrinsically deformable properties of LM allow to achieve more tuning states [19]. Liquid metal (LM) can be used to create switches [17], [18] or to reconfigure the radiating element [19], [20], [21], [22], [23], [24], [25], [26]. A LM-based antenna can also be fabricated with soft materials for wearable and flexible applications [27], [28], and has gained much interest in reconfigurable antennas. [17] presents a circular patch antenna incorporating a C-shaped slot. The polarization state is altered by repositioning the LM in the slot. In [20], five discrete polarization states can be generated by actuating the LM based dipole. However, its radiation patterns are affected by changing the polarization. In [19], [22], and [23], the polarization is reconfigured by moving LM within the slots of a rectangular patch. References [24] and [25] presents a PRA with a square slot and microchannels. LP, LHCP and RHCP are realized by filling or emptying the channels with LM [24], [25]. In [26], the polarizations can be switched among LPs and CPs when LM serves as switches to open/close the slots etched on the crossed bowtie dipole antennas. For most of the reported designs where LM is employed to reconfigure the polarization of an antenna, reconfiguration is achieved by altering the radiating element. This means each element in a high-gain array needs to be tunned with LM, which greatly increases the complexity in both manufacture and implementation. Altering the radiating elements also often has the unintended consequence of modifying other parameters, such as the operating frequency or radiation pattern [17].

To overcome these problems, a polarization reconfigurable patch array is proposed in this paper using a novel reconfiguration mechanism only enabled by the use of the liquid metal, EGaIn. The array can switch between vertical polarization (VP), horizontal polarization (HP), LHCP, and RHCP by employing a reconfigurable feed network.

The key features of the antenna and the main contribution of the work include: (1) A functionally reconfigurable coupler that can switch between a 90° hybrid coupler and a crossover. This is achieved by physically changing the width of the microstrip transmission lines, which is only made possible by using LM contained in microfluidic channels. Although it is not implausible, it would be more complicated and require different circuit topologies to realize similar reconfiguration using PINs or other tuning techniques. (2) A low-loss (0.27 dB) and high-isolation (50 dB) double-pole-double-throw (DPDT) switch with matched termination on unused ports, again using LM; (3) An array antenna that employs the reconfigurable feed network to alter its polarisation state without disturbing the radiating elements. The same reconfigurable feed network can also be applied to larger arrays without necessarily increasing the complexity of the tuning. This is another major advantage of the proposed reconfiguration scheme.

Section II introduces the scheme for reconfiguring the polarization of the antenna. The LM-based reconfigurable coupler and the DPDT switch are studied in Section III. Section IV presents the polarization reconfigurable array. Section V shows the fabrication and measurement. Section VI discusses switching speed and power handling, and Section VII draws a conclusion.

II. Reconfigurable Feed Network for Multi-Polarization Antennas

Fig. 1 illustrates the proposed reconfigurable feed network and the operating mechanism of the polarization reconfigurable antenna. The radiation element is formed from a microstrip patch antenna incorporating two feed points. Polarization reconfiguration is achieved by using a reconfigurable feed network. This approach avoids disturbing the radiating element. The feed is composed of a reconfigurable coupler and a switch. It could also be described as a switched reconfigurable coupler. For State-I (RHCP) and II (LHCP) (See Fig. 1), the coupler operates as a 3-dB 90° hybrid, providing 90° phase difference between the two outputs. These are used to feed the patch and excite circular polarization. Depending on the state of the DPDT switch, RHCP or LHCP can be excited as State-I or II. To switch from the CP states to the LP states (i.e., States III (HP) and IV (VP)), the 3-dB hybrid has to be reconfigured to operate as a crossover. Under this state, the patch is only actively fed from one feed point whereas the other feed point is isolated and loaded. This functional reconfiguration between a coupler and a crossover is achieved by the use of LM. The two LP states can be selected by the DPDT switch. In all cases, the unused ports should ideally be terminated with matched loads. This is indeed made possible by the LM-enabled switch, as will be discussed later. Mercury (Hg) has very limited applications due to its high toxicity. The most used LM material is the non-toxic gallium-based alloy such as eutectic gallium-indium (EGaIn), featuring a Ga:In weight ratio of 75.5:24.5, a melting point of 15.5°C and conductivity of 3.4×10^6 S/m [29]. EGaIn has the merits of a low melting point, low toxicity, low viscosity, and exceptional electrical, flow, and self-healing properties [29]. Hence, EGaIn is utilized in the proposed design. Next, we will discuss each component of the antenna sub-system.

TABLE I
GEOMETRIES OF THE PROPOSED RECONFIGURABLE COUPLER (UNIT: MM)

Wc_0	Wc_1	Wc_2	Wc_{2c}	Wc_3	Wc_{3c}	Lc_1	Lc_2
1.62	2.65	0.39	1.62	2.05	3.39	15.2	14.5

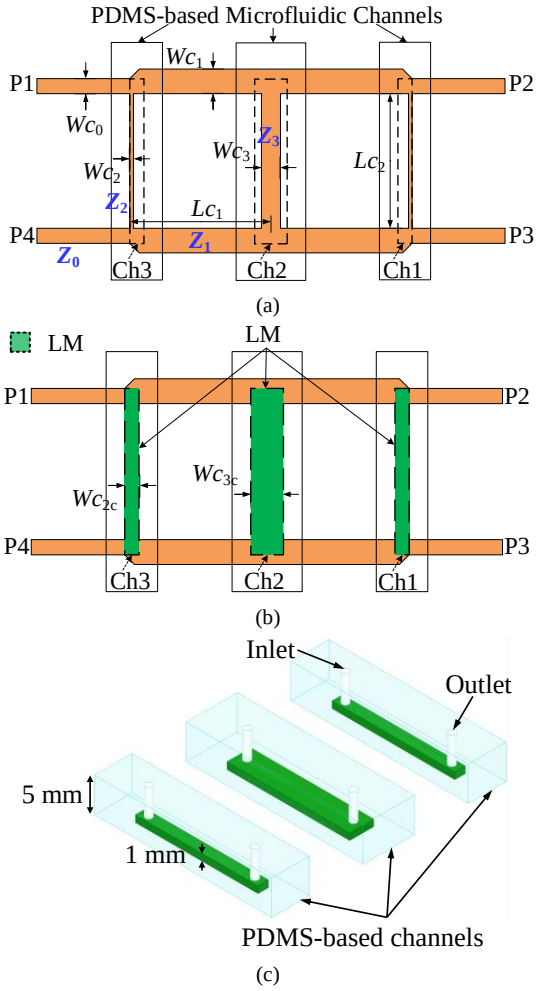

Fig. 2. Baseline schematic of the reconfigurable coupler. (a) State A: 3-dB 90º directional coupler. (b) State B: crossover. (c) Microfluidic channels.

III. LM-ENABLED SWITCHED RECONFIGURABLE COUPLER

The key innovation in this work is the reconfigurable coupler that can switch between two circuit functions: a coupler or a crossover. A microstrip coupler is a phased power-combining/dividing device, widely utilized in antenna feed networks [30]. Fig. 2 presents a two-section branch-line coupler. The transmission characteristics of the branch-line coupler are determined by the characteristic impedances of the branch lines. Hence, reconfiguration can be achieved by changing the impedances of the branch lines, while maintaining their electrical length (λ/4). The latter requirement is critical. It is not easy to use conventional techniques (e.g. varactors) to realize the same 'mode' of reconfiguration. In [31], a reconfigurable power-dividing ratio (PDR) is achieved by adjusting the varactors loaded in a patch hybrid coupler. However, equivalent phase shift through the structure also changes with the PDR, causing deterioration of isolation and matching. It is a common problem. A row of varactor diodes could be loaded to the branch line to change their distributed capacitance and therefore the characteristic impedance. However, this would also decrease the electrical length. The line sections would no longer be a quarter wavelength, not meeting the impedance matching condition of the coupler or the crossover. Uniquely, liquid metals, with its fluidic and shape shifting properties, can be used to directly alter the width of the branch lines, without changing their electrical lengths, and therefore reconfigure the branch-line coupler, without deterioration of the isolation or matching. This characteristic enables the functional reconfiguration as will be discussed next.

The proposed reconfigurable branch-line coupler is demonstrated in Fig. 2. The substrate is Taconic TLY-5 (ε_r = 2.2, tanδ = 0.0009, and h = 0.508 mm). Shown in Fig. 2(a) is the 3-dB 90° directional coupler, designed to achieve the circularly polarized excitation. The S-parameters of the three-section branch-line coupler can be calculated based on even- and odd-mode method. By using transmission ABCD matrixes [32], the even-mode and odd-mode ABCD matrixes can be expressed as follows:

$$\begin{bmatrix} A_E & B_E \\ C_E & D_E \end{bmatrix} = \begin{bmatrix} 1 & 0 \\ j\overline{Y}_2 & 1 \end{bmatrix}\begin{bmatrix} 0 & j\overline{Z}_1 \\ j\overline{Y}_1 & 0 \end{bmatrix}\begin{bmatrix} 1 & 0 \\ j\overline{Y}_3 & 1 \end{bmatrix}\begin{bmatrix} 0 & j\overline{Z}_1 \\ j\overline{Y}_1 & 0 \end{bmatrix}\begin{bmatrix} 1 & 0 \\ j\overline{Y}_2 & 1 \end{bmatrix}$$
$$= \begin{bmatrix} -1+\overline{Z}_1^2\overline{Y}_2\overline{Y}_3 & -j\overline{Z}_1^2\overline{Y}_3 \\ jY_2(-2+\overline{Z}_1^2\overline{Y}_2\overline{Y}_3) & -1+\overline{Z}_1^2\overline{Y}_2\overline{Y}_3 \end{bmatrix} \quad (1)$$

$$\begin{bmatrix} A_o & B_o \\ C_o & D_o \end{bmatrix} = \begin{bmatrix} 1 & 0 \\ -j\overline{Y}_2 & 1 \end{bmatrix}\begin{bmatrix} 0 & j\overline{Z}_1 \\ j\overline{Y}_1 & 0 \end{bmatrix}\begin{bmatrix} 1 & 0 \\ -j\overline{Y}_3 & 1 \end{bmatrix}\begin{bmatrix} 0 & j\overline{Z}_1 \\ j\overline{Y}_1 & 0 \end{bmatrix}\begin{bmatrix} 1 & 0 \\ -j\overline{Y}_2 & 1 \end{bmatrix}$$
$$= \begin{bmatrix} -1+\overline{Z}_1^2\overline{Y}_2\overline{Y}_3 & j\overline{Z}_1^2\overline{Y}_3 \\ -jY_2(-2+\overline{Z}_1^2\overline{Y}_2\overline{Y}_3) & -1+\overline{Z}_1^2\overline{Y}_2\overline{Y}_3 \end{bmatrix} \quad (2)$$

where $\overline{Z}_1 = Z_1/Z_0$, $\overline{Y}_1 = Z_0/Z_1$, $\overline{Y}_2 = Z_0/Z_2$, and $\overline{Y}_3 = Z_0/Z_3$.

Then, the even-mode (S^E) and odd-mode (S^O) S-parameters can be calculated by using the corresponding ABCD matrixes [32].

$$S_{11}^E = \frac{A_E+B_E-C_E-D_E}{A_E+B_E+C_E+D_E} \quad (3)$$
$$S_{21}^E = \frac{2}{A_E+B_E+C_E+D_E} \quad (4)$$
$$S_{11}^o = \frac{A_o+B_o-C_o-D_o}{A_o+B_o+C_o+D_o} \quad (5)$$
$$S_{21}^o = \frac{2}{A_o+B_o+C_o+D_o} \quad (6)$$

According to equations (1)-(6), the S-parameters of the coupler can be expressed as follows [32]:

$$S_{11} = \frac{1}{2}(S_{11}^E + S_{11}^o) = \frac{\overline{Z}_1^4\overline{Y}_3^2-\overline{Y}_2^2(4-4\overline{Z}_1^2\overline{Y}_2\overline{Y}_3+\overline{Z}_1^4\overline{Y}_2^2\overline{Y}_3^2)}{Q} \quad (7)$$
$$S_{21} = \frac{1}{2}(S_{21}^E + S_{21}^o) = \frac{4(-1+\overline{Z}_1^2\overline{Y}_2\overline{Y}_3)}{Q} \quad (8)$$
$$S_{31} = \frac{1}{2}(S_{21}^E - S_{21}^o) = \frac{2j(\overline{Z}_1^2\overline{Y}_3+2\overline{Y}_2-\overline{Z}_1^2\overline{Y}_2^2\overline{Y}_3)}{Q} \quad (9)$$
$$S_{41} = \frac{1}{2}(S_{11}^E - S_{11}^o) = \frac{-2j(-1+\overline{Z}_1^2\overline{Y}_2\overline{Y}_3)(\overline{Z}_1^2\overline{Y}_3-2\overline{Y}_2+\overline{Z}_1^2\overline{Y}_2^2\overline{Y}_3)}{Q} \quad (10)$$
$$Q = 4(-1+\overline{Z}_1^2\overline{Y}_2\overline{Y}_3)^2 + (\overline{Z}_1^2\overline{Y}_3+2\overline{Y}_2-\overline{Z}_1^2\overline{Y}_2^2\overline{Y}_3)^2 \quad (11)$$

As for the directional coupler, the S-parameters should satisfy:

$$|S_{21}| = |S_{31}| = \frac{1}{\sqrt{2}} \quad (12)$$
$$\angle S_{21} - \angle S_{31} = 90^o \quad (13)$$
$$|S_{41}| = 0 \quad (14)$$

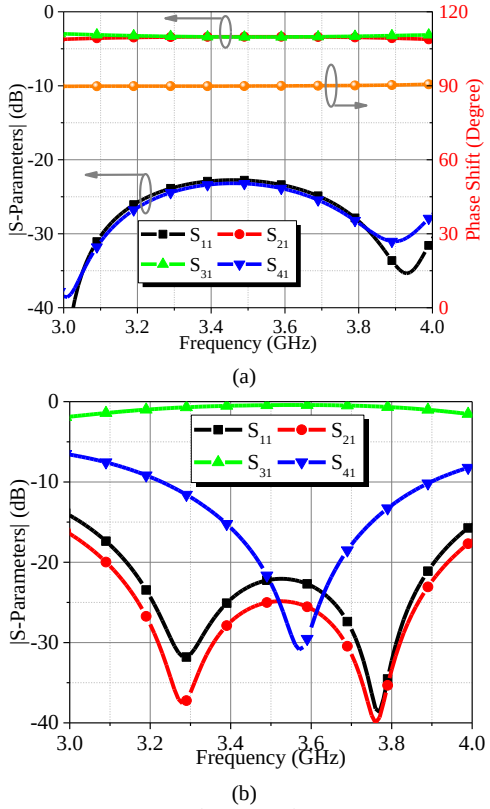

Fig. 3. Simulated S-parameters of the reconfigurable coupler. (a) State A: 3-dB 90º directional coupler. (b) State B: crossover.

Substituting (8) and (9) into (12), and substituting (14) into (10), the following equations can be obtained:

$$Z_2 = Z_0(\sqrt{2}+1) \tag{15}$$

$$Z_3 = \sqrt{2}\frac{Z_1^2}{Z_0} \tag{16}$$

According to equations (15) and (16), Z_2 = 120.7 Ω and Z_3 = 40.8 Ω can be obtained when Z_0 = 50 Ω and Z_1 = 38 Ω. The optimized dimensions are listed in Table I, and the corresponding simulation results are shown in Fig. 3(a). The coupler has a good amplitude balance (S_{21} = -3.37 dB, and S_{31} = -3.41 dB) and 89.9º phase difference ($\angle S_{21}$-$\angle S_{31}$) at 3.5 GHz, which provides a circularly polarized excitation for the dual-fed radiating element. Due to the symmetry of the coupler, when the feed port is switched from P1 to P4, the phase difference at the output changes its sign to -90º. This is used to switch the sense of circular polarization.

To realize the linearly polarized excitation, we need to suppress one of the outputs from the coupler. This is achieved by reconfiguring the 90° coupler to operate as a crossover. To reduce the design complexity in this functional reconfiguration, the impedance (Z_1) of the series branches is kept unchanged, while those of the three parallel branches are optimized for the characteristics of the crossover. For the crossover, the S-parameters should satisfy $|S_{21}|$ = 0 and $|S_{31}|$ = 1. This means $\overline{Z}_1^2\overline{Y}_2\overline{Y}_3$ = 1 according to (8). Substituting $\overline{Z}_1^2\overline{Y}_3 = 1/\overline{Y}_2$ into (9) and (11), $\overline{Y}_2 = 1$ can be obtained. Hence, the impedances (Z_2 and Z_3) for the crossover should satisfy the following equations:

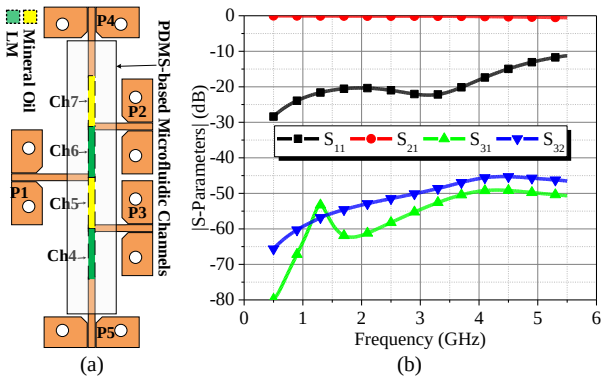

Fig. 4. DPDT switch. (a) Layout and (b) simulated results.

$$Z_2 = Z_0 = 50\ \Omega \tag{17}$$

$$Z_3 = \frac{Z_1^2}{Z_0} = 28.88\ \Omega \tag{18}$$

EGaIn is used to physically increase the line widths of the three parallel branches and convert their impedances (Z_2 and Z_3) into $Z_2 = 50\ \Omega$ and $Z_3 = 28.88\ \Omega$, which allows the device to operate as a signal crossover with a high isolation of 25 dB.

To implement the 'switching' of the line widths, LM is injected into a series of microfluidic channels, marked out in Fig. 2, formed from polydimethylsiloxane (PDMS). PDMS, an elastomeric material, enables inexpensive and quick microfabrication alongside dense integration, allowing intricate fluid manipulation. The dielectric constant of PDMS is around 2.67, and its loss tangent is 0.0375 at 77 GHz [29]. The thickness of PDMS may affect the characteristic impedances of the microstrip lines. To minimize the impact of PDMS on device performance while ensuring channel functionality, the height of PDMS is chosen to be 5 mm. The height of the channel is 1 mm. There is a 2 mm-wide margin of PDMS around the channel. To avoid the leakage of LM, the PDMS channels are bonded to the PCB board using the plasma bonding method [33], [34], which enables bonding between microfluidic channels and PCB board. These channels sit on the top of the parallel lines in the coupler. Note that the effect of the PDMS material has been considered in the simulation and design, aiming to minimize the channel impact on the device performance. As shown in Fig. 2(a) and Fig. 3(a), when the LM is emptied from microfluidic channels, the coupler operates as a 3-dB 90º directional coupler, in State A. When the microfluidic channels are filled with LM, the widths of the parallel branches are changed, and the coupler turns into a crossover (State B), as presented in Fig. 2(b). This is a novel reconfiguration mechanism that is only made possible using LM.

From (17) and (18), the initial widths of the transmission lines are W_{c2c} = 1.62 mm and W_{c3c} = 3.28 mm. After optimization, W_{c2c} and W_{c3c} are set to 1.62 and 3.39 mm. The simulated results of the crossover are plotted in Fig. 3(b). The simulated insertion loss ($|S_{31}|$) is about 0.44 dB, and the isolation ($|S_{21}|$) is better than 25 dB.

To switch between the two input ports of the coupler, a DPDT switch with two matched ports is designed, as shown in Fig. 4(a). The DPDT will switch between the input port (P1) and two output ports (P2 and P3), while P4 and P5 are terminated with a matched load. Firstly, Ch4, Ch5, Ch6, and Ch7 are sequentially filled with LM, mineral oil, LM, and

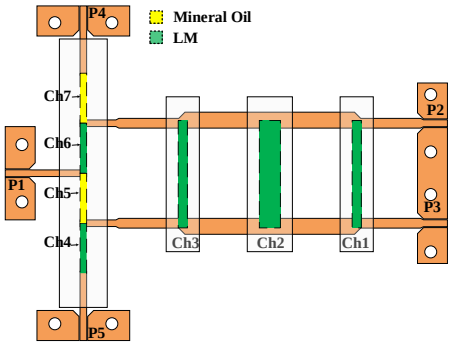

Fig. 5. Reconfigurable coupler with DPDT switch.

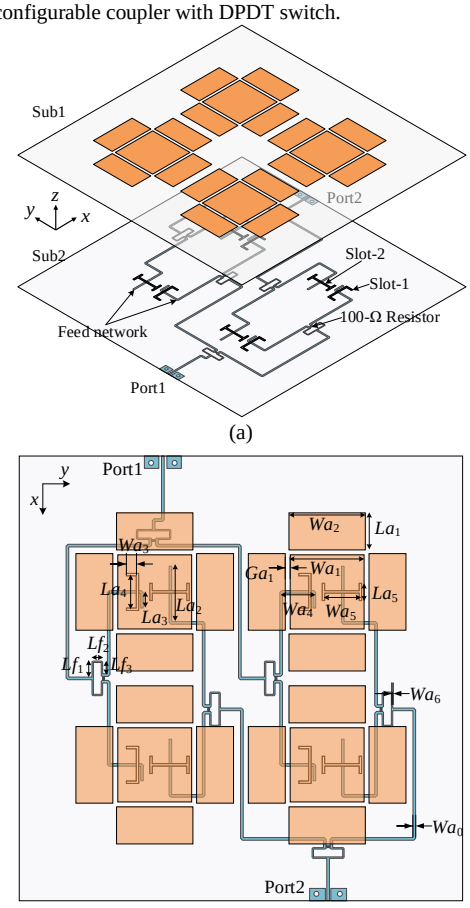

Fig. 6. Quad-polarization antenna array. (a) 3D view. (b) Top view.

TABLE II
GEOMETRIES OF QUAD-POLARIZATION PATCH ARRAY (UNIT: MM)

Wa_0	Wa_1	Wa_2	Wa_3	Wa_4	Wa_5	Wa_6	Ga_1
1.07	30	31	5	12.43	14	0.57	0.5
La_1	La_2	La_3	La_4	La_5	Lf_1	Lf_2	Lf_3
15	22.4	6	13	7	6.43	3.18	4.56

mineral oil. In the case illustrated in Fig. 4, P2 is connected to P1 (On state), while P3 (Off state) is matched. Conversely, when the two slugs of LM are pushed across to fill Ch5 and Ch7, P3 is connected to P1 (On state), while P2 (Off state) is terminated. This way, the unused ports are always matched, during switching. The simulated insertion loss (IL) in the ON state is 0.27 dB, and the isolation is higher than 50 dB, which is difficult to achieve using PIN diodes. For example, if we use a pair of MA4AGP907 PIN diodes (widely used in RF switches)

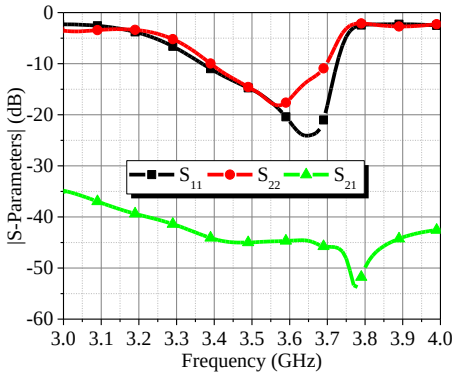

(a)

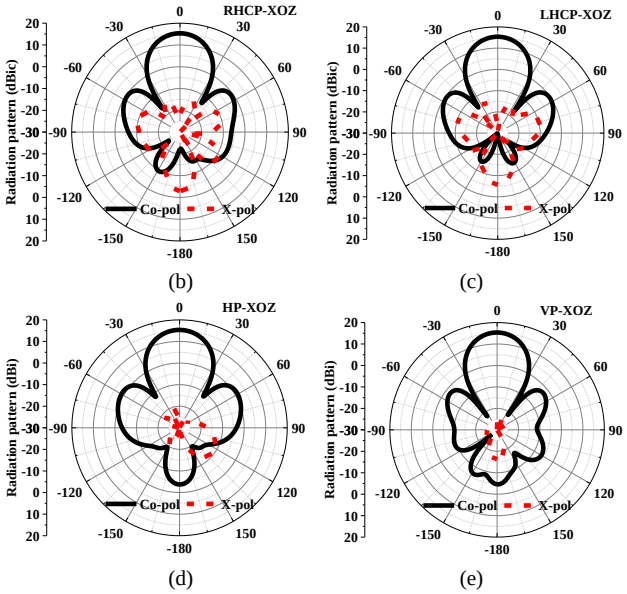

(b) (c) (d) (e)

Fig. 7. Simulated results of quad-polarization patch array. (a) $|S_{11}|$. (b) State-1 (RHCP). (c) State-2 (LHCP). (d) State-3 (HP). (e) State-4 (VP).

to realize the same switch function, the simulated insertion loss would be 0.72 dB and the isolation is around 22.7 dB.

The switched reconfigurable coupler as a whole is presented in Fig. 5. There are four states. Due to the symmetry of the structure, the responses of only two states of the coupler and crossover are shown in Fig. 9(a) and (b). Simulation shows the switch has little impact on the performance of the coupler after cascading the two components. When LM is emptied from Ch1, Ch2 and Ch3, the coupler operates as a 3-dB 90º directional coupler. When Ch4 and Ch6 are filled with LM, P2 and P3 have almost the same amplitude ($|S_{21}|$= -3.34 dB, $|S_{31}|$= -3.44 dB at 3.5 GHz), and a 90º phase difference ($\angle S_{21}$-$\angle S_{31}$). When Ch5 and Ch7 are filled with LM, P2 and P3 have almost the same amplitude, but a -90º phase difference ($\angle S_{21}$-$\angle S_{31}$). When Ch1, Ch2, and Ch3 are fully filled with LM, the coupler operates as a crossover. When Ch4 and Ch6 are filled with LM, P3 is the pass-through port ($|S_{31}|$ = 0.53 dB at 3.5 GHz) and P2 is the isolated port ($|S_{21}|$ = 18.6 dB at 3.5 GHz). When Ch5 and Ch7 are filled with LM, P2 becomes the pass-through port and P3 is the isolated port. After being cascaded with the switch, the directional coupler still shows a good amplitude balance ($|S_{21}|$ = -3.34 dB and $|S_{31}|$ = -3.44 dB at 3.5 GHz) and 90º phase difference, and the crossover has good transmission (0.53 dB at 3.5 GHz) and isolation characteristics (over 18.6 dB).

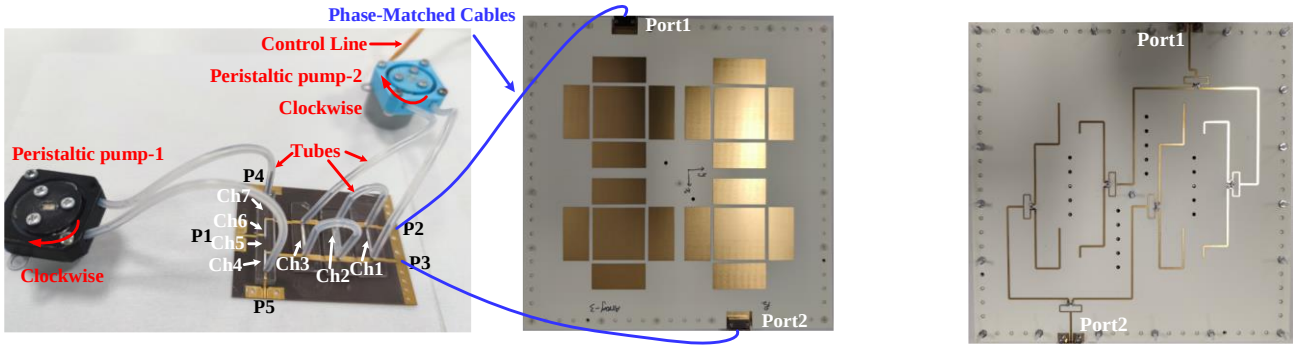

(a) (b)

Fig. 8. Fabricated prototypes. (a) Top view cascaded with switched reconfigurable coupler and (b) bottom view of 2×2 array.

IV. Polarization Reconfigurable Array

Dual-fed patch antennas are often used to create antennas capable of supporting two polarization states [35], [36], [37], [38], [39]. Generally, the gain of the dual-polarized radiating element is only about 7 dBi [35], [36], [37]. To improve the gain, arrays are normally formed. However, a large feed network would cause increased insertion loss and therefore reduce the antenna efficiency [36], [37], [38], [39]. In this paper, four parasitic elements, coupled to the primary radiator, are utilized to enhance the gain of the radiating element, as shown in Fig. 6. The realized gain of the radiator element increases by about 3 dB due to the use of four parasitic elements.

The 2×2 array consists of two 2-stage Wilkinson power dividers, 8 coupling slots, and 4 radiating elements. The array is printed on the upper surface of Sub1, the coupling slots are etched on the upper surface of Sub2, and the power dividers are printed on the lower surface of Sub2. Six 100-Ω resistors are used to absorb the reflected power and improve the isolation between the coupling slots. The air gap between Sub1 and Sub2 is h_{gap2} = 2.5 mm. Both Sub1 and Sub2 are Rogers RO4350 substrate with a thickness of 0.508 mm.

When the input is applied at Port1, all the Slot-1s are excited in such a way that the array radiates with HP. When the input is applied at Port2, all the Slot-2s are excited, causing the array to radiate with VP. The electrical lengths of the two power dividers are optimized to keep the slots excited in phase. The dimensions are listed in Table II. The simulated results for the array are shown in Fig. 7. The 10-dB impedance bandwidth is 9.4% (3.35-3.68 GHz), and the isolation level is better than 42 dB in the operating frequency band. As demonstrated in Fig. 7(b)-(e), four polarizations are realized by switching the amplitude and phase of P1 and P2. The simulated realized gain is higher than 15.4 dBi/dBic, and the AR of the RHCP and LHCP is less than 0.24 dB.

V. Fabrication and Measurement

As shown in Fig. 8, the 2×2 array and the switched reconfigurable coupler are all fabricated by PCB technology. The PDMS microfluidic channels are fabricated from 3D printed mould composed of Ultimaker tough PLA (polylactic acid) materials. The PDMS channels are connected by tubes for ease of actuation. As shown in Fig. 8(a), two peristaltic pumps are utilized for the actuation, for their ability to control the movement of LM in both directions. The pumps were 3D printed and used a stepper motor (28BYJ-48). Firstly, mineral oil (colorless and odorless) passes through the microfluidic channels to form a very thin film coating on the walls, which prevents the LM from sticking to the walls. Then the LM and mineral oil are pumped into the channels and tubes. Mineral oil serves as a sealant to the LM and an effective insulator. The loss tangent of mineral oil is very small. So, the influence of the mineral oil is negligible, and it has been verified by the measurement.

TABLE III
States of the Reconfigurable Coupler With DPDT Switch

Operating state	State-1	State-2	State-3	State-4
Ch1, Ch2 and Ch3	OFF		ON	
Circuit type	Directional coupler		Crossover	
Ch4 and Ch6	ON	OFF	ON	OFF
Ch5 and Ch7	OFF	ON	OFF	ON
Polarization	RHCP	LHCP	HP	VP
Gain (dBi/dBic)	14.54	14.23	15	14.66
Radiation Efficiency	87.5%	82.8%	90.6%	87%
AR (dB)	1.03	0.47	N.A.	N.A.
3 dB-AR beamwidths	61°	61°	N.A.	N.A.

For the DPDT switch (indicated by ports P1, P4, and P5 on the left-hand side of the circuit in Fig. 8(a)), when the peristaltic pump-1 rotates clockwise, the LM droplets in Ch7 and Ch5 will be pushed towards P5 to bridge Ch6 and Ch4 respectively. Reversely, the LM droplets will move back to Ch7 and Ch5 when the peristaltic pump-1 rotates anticlockwise. For the reconfigurable coupler shown on the right-hand side of the circuit, when the peristaltic pump-2 rotates clockwise, the LM droplets in Ch1, Ch2, and Ch3 will be emptied and moved into the tubes. When the peristaltic pump-2 rotates anticlockwise, the LM droplets will be pushed back to Ch1, Ch2, and Ch3 from the tube. The vertical line sections in the coupler will be defined by the liquid metals in the microfluidic channels Ch1, Ch2, and Ch3. In this way, the widths of the microstrip lines are physically changed to enable the functional switch between a hybrid coupler and a crossover. This is a feature that would be difficult or impossible to implement using PINs or other tuning

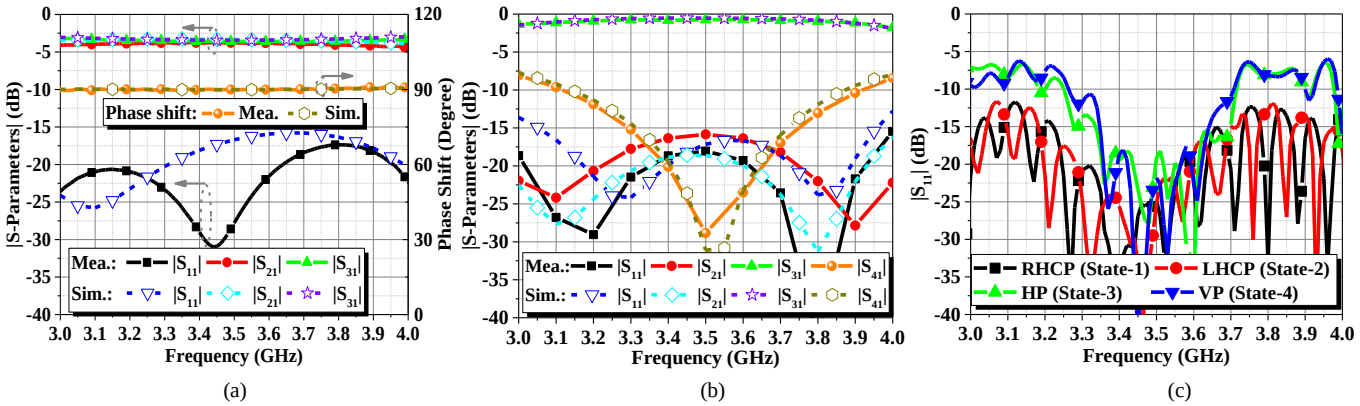

Fig. 9. Measurement |S-parameters|: (a) State-1 (RHCP) and (b) State-3 (HP) of the reconfigurable coupler with DPDT switch. (Solid symbol: Measured results; Hollow symbol: Simulated results.) (c) Four states of the quad-polarization 2×2 array.

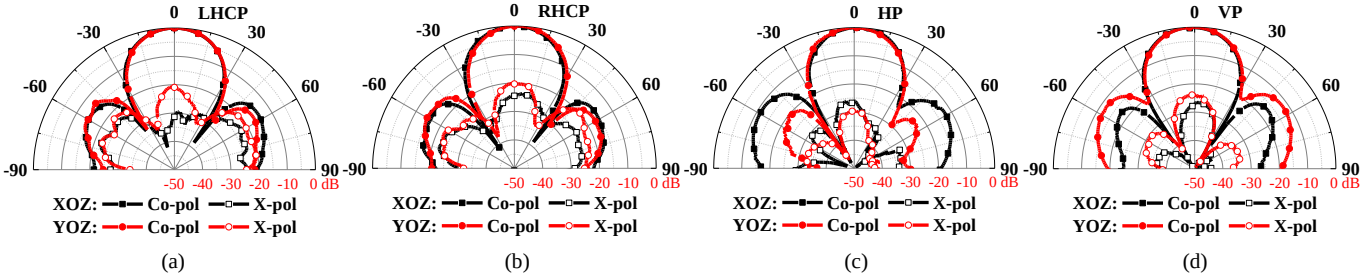

Fig. 10. Radiation patterns at 3.5 GHz of quad-polarization 2×2 array. (a) State-1 (RHCP), (b) State-2 (LHCP), (c) State-3 (HP), and (d) State-4 (VP).

mechanisms. The operation states of the coupler and the switch are summarized in Table III.

The switched reconfigurable coupler in Fig. 8(a) was first tested. Fig. 9 shows the measured results. Considering the symmetry of the circuit, only two states are shown in Fig. 9(a) and (b). In State-1 (RHCP), as shown in Fig. 9(a), the amplitude imbalance is about 0.2 dB ($|S_{21}|$ = -3.51 dB, $|S_{31}|$ = -3.71 dB), the transmission efficiency (η_{co}) of the coupler is about 93.2%, and the phase difference ($\angle S_{21}$-$\angle S_{31}$) is 89.95° at 3.5 GHz. Similarly, excellent amplitude balance and 90° phase shift are achieved for State-2 (LHCP). In State-3 (HP) when the coupler is reconfigured into a crossover, as presented in Fig. 9(b), the IL of the through path between P_1 and P_3 is about 0.7 dB. The isolation level ($|S_{21}|$) of the crossover is higher than 15 dB over 3.3-3.7 GHz. Only the radiation patterns at the central frequency of 3.5 GHz are shown. There is no obvious degradation of the radiation performance at other frequencies over the bandwidth. The transmission efficiency (η_{cr}) of the crossover is around 92.3%. Overall, the measured transmission efficiency of the switched reconfigurable coupler is better than 92% at 3.5 GHz.

The 2×2 array and the switched reconfigurable coupler in Fig. 8 are interconnected using phase-matched cables and measured. The measurement results are summarized in Table III. Fig. 9(c) shows the overlapping impedance bandwidth is 13.2% (3.25 - 3.71 GHz). The radiation patterns of the four polarization states are shown in Fig. 10. The realized gain is better than 14.23 dBi/dBic at 3.5 GHz, the peak total radiation efficiency of the circular polarizations is 87.3% at 3.5 GHz, and the ARs of the circular polarizations are about 1.0 dB (RHCP) and 0.5 dB (LHCP), respectively. The RHCP properties at the XOZ plane are plotted in Fig. 11. The measured realized gain is

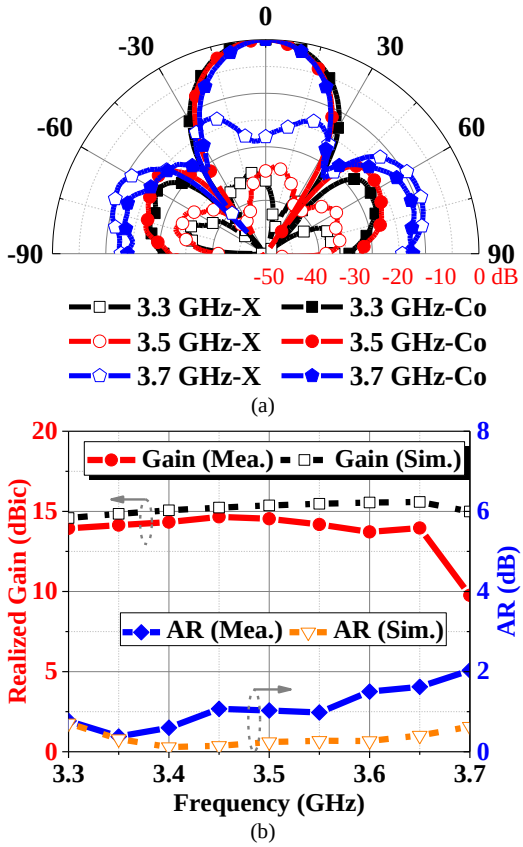

Fig. 11. Measurement results of the RHCP at XOZ plane as a function of frequency. (a) Radiation patterns. (b) Realized gain and AR.

higher than 13.7 dBic over 3.3-3.65 GHz, and the AR is lower than 2.03 dB within 3.3-3.7 GHz (11.4% FBW). The measurement results verify that the proposed reconfigurable coupler can be used to excite multiple polarizations.

TABLE IV
PERFORMANCE COMPARISON AMONG POLARIZATION RECONFIGURABLE PLANAR PATCH ANTENNAS

Ref.	f_0 (GHz)	Overlapped Impedance BW	AR BW	Polarizations	Peak CP Gain (dBic)	Reconfigurable Part	Method
[3]	2.43	17.7%	4%	HP, VP, LHCP, RHCP	8	Radiator	PINs
[5]	3.92	3.1%	3.20%	LP, LHCP, RHCP	10.6	Radiator	PINs
[22]	2.45	23.2%	2.08%	LP, LHCP, RHCP	7.33	Radiator	LM
[23]	3.43	8.1%	5.83%	LHCP, RHCP	10.54 (2×8 array)	Radiator	LM
[24]	2.16	-	20.55%	LP, LHCP, RHCP	3.97	Radiator	LM
[25]	5.65	22.9%	39.2%	LP, LHCP, RHCP	3.8	Radiator	LM
This Work	**3.48**	**13.2%**	**11.43%**	**HP, VP, LHCP, RHCP**	**14.66 (2×2 array)**	**Feed network**	**LM**

In Table IV, the performance of the proposed antenna has been compared with that of multi-polarized planar patch antennas in the literature. Firstly, it is important to note that none of the previous polarization reconfigurable antennas used a similar reconfiguration approach as reported in this work. The radiating element used in this work offers higher gain than other designs [3], [5], [22], [23], [24], [25], attributed to the use of parasitic elements. Polarization reconfiguration has been achieved entirely by using a reconfigurable feed network (the LM-based switched reconfigurable coupler), without disturbing the radiating elements, making it a good option for high-gain polarization-reconfigurable antenna arrays. Most of the references only have two or three polarizations (LP, LHCP, and RHCP) [5], [22], [23], [24], [25], while the proposed design has four polarizations (HP, VP, LHCP, and RHCP). In addition, the AR bandwidth of the proposed antenna is better than that of most of the reported antennas [3], [5], [22], [23]. Another advantage of the proposed reconfiguration scheme, based exclusively on a reconfigurable feed network, is that it is readily scalable to larger arrays without necessarily increasing the complexity. In addition, the AR bandwidth of the proposed antenna is better than that of most of the reported antennas [3], [5], [22], [23]. It is also important to note that none of the previous polarization reconfigurable antennas used a similar reconfiguration approach as reported in this work.

VI. DISCUSSION

A primitive actuation method with peristaltic pumps is used in this work. As a relatively new and 'unusual' tuning method, the effectiveness of LM tuning still has a long way to go to be comparable with other electrically tuning methods. A main challenge is the need for more compact and accurate tuning mechanisms and with a decent switching speed. The pump-based or pneumatic/hydraulic-based tunning method, as used in this case, is bulky. However, there is scope for miniaturization by using micropumps, more microfluidics or MEMS-based techniques such as the one shown in [40]. New electrical or magnetic actuation methods being developed by other communities [29] may be adapted to our field too.

It is known that LM has a limitation on its tuning speed. It is in milli-seconds using existing actuation techniques, which is not comparable to diodes. Using known actuation techniques, it may never compete with PINs. For the peristaltic pump used in this work, the measured switching speed of the DPDT is about 1 s. There is some scope to reduce the switch time under the current setup by changing the parameters of the pump as well as the size of the tubes and the microfluidic channels.

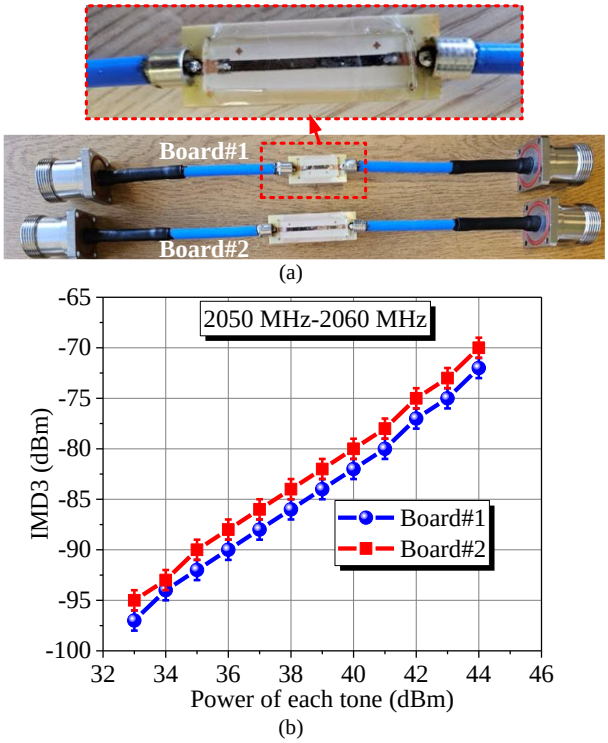

Fig. 12. High power investigation of the LM-based microstrip lines. (a) Sample assembly. The lengths of LM in Board #1 and 2 are 20 and 40 mm, respectively. (b) Third-order intermodulation distortion (IMD3) measurement versus input power.

As for the power handling, the liquid metal switch should have some advantages here due to its passive nature. We have not tested the power handling on the functional devices presented in this paper due to constraints in our high-power measurement capability. However, we did high-power testing on liquid-metal microstrip lines, where there are two contact points between liquid metals and the copper lines, as shown in Fig. 12(a). It has been suspected these junctions between the liquid metal and the copper track could be a source of

nonlinearity. For testing, notably, the board has been soldered to a tin-plated solid copper transition unit, which is connected to a PIM (passive intermodulation)-certified cable assembly and DIN 7/16 connector. The frequency of the IMD3 (Two-tone third-order intermodulation distortion) measurement falls within the range of 2050 MHz to 2060 MHz. The measurement shows the transmission line can endure 47 dBm (50 W) (limited by the equipment) without problems. Its linearity is also very good, as shown in Fig. 12(b), at least not worse than the used SMA connectors. We still cannot draw a definite conclusion here and have planned to perform more high-power measurements on the reconfigurable devices using specialist equipment.

VII. Conclusion

This paper has proposed a novel switched reconfigurable coupler as the reconfigurable feed network for multi-polarization antennas. By changing the widths of the parallel microstrip branches, only enabled by the use of liquid metals, the coupler can be switched between a 3-dB 90º directional coupler and a crossover. An LM-based DPDT switch has been designed to switch the input port of the reconfigurable coupler. Together they form the reconfigurable feed network, rendering four different polarization states. Most of the previous work on multi-polarization antennas requires the reconfiguration of each radiating element. In our design, instead, it is only necessary to reconfigure the feed network without disturbing the radiation element. Hence, a larger array will not necessarily increase the complexity of the tuning using the LM-based reconfiguration scheme. This is an important feature that simplifies the fabrication and reduces operational complexity. The LM-based reconfigurable coupler and switch can be employed in other multi-functional circuits and antennas. The reconfigurable coupler itself could be extended into other multi-functional signal distribution networks such as frequency-reconfigurable couplers, ratio-reconfigurable power dividers, or even reconfigurable Butler matrices.

It is worth noting that practical handling of liquid metals still faces several challenges. Gallium readily forms alloys with some metals commonly used in electronics, e.g., copper and aluminum. On the one hand, this aids in improving the interconnection between LM and normal conductors. On the other hand, this poses the risk of circuit corrosion. Fortunately, EGaIn typically does not induce significant corrosion on copper. In fact, LMs based on gallium are generally compatible with copper and can form a protective oxide layer on the copper surface, which helps prevent further corrosion. Another potential difficulty with LMs is that remnants of LM often stick to the microfluidic channels due to the oxide layer's high wettability. This can be addressed by employing mineral oil or an electrolyte, such as sodium hydroxide solution. Finally, LM has superb electrical and thermal conductivities. On the one hand, the expansion of LM with rising temperature could impact the stability of the device; On the other hand, its thermal conductivity could be harnessed to enhance heat dissipation or to actuate LM.

Acknowledgment

For the purpose of open access, the author(s) has applied a Creative Commons Attribution (CC BY) license to any accepted manuscript version arising.

References

[1] R. Alhamad, E. Almajali, and S. Mahmoud, "Electrical reconfigurability in modern 4g, 4g/5g and 5g antennas: A critical review of polarization and frequency reconfigurable designs," *IEEE Access*, vol. 11. pp: 29215-29233, Mar. 2023. doi: 10.1109/access.2023.3260073.

[2] V. T. Bharambe, J. Ma, M. D. Dickey, and J. J. Adams, "Reshape: A liquid metal-based reshapable aperture for compound frequency, pattern, and polarization reconfiguration," *IEEE Trans. Antennas Propag.*, vol. 69. no. 5, pp: 2581-2594, May 2021. doi: 10.1109/tap.2020.3037803.

[3] K. M. Mak, H. W. Lai, K. M. Luk, and K. L. Ho, "Polarization reconfigurable circular patch antenna with a c-shaped," *IEEE Trans. Antennas Propag.*, vol. 65. no. 3, pp: 1388-1392, Mar. 2017. doi: 10.1109/tap.2016.2640141.

[4] S.-L. Chen, F. Wei, P.-Y. Qin, Y. J. Guo, and X. Chen, "A multi-linear polarization reconfigurable unidirectional patch antenna," *IEEE Trans. Antennas Propag.*, vol. 65. no. 8, pp: 4299-4304, Aug. 2017. doi: 10.1109/tap.2017.2712185.

[5] Q. Chen, J.-Y. Li, G. Yang, B. Cao, and Z. Zhang, "A polarization-reconfigurable high-gain microstrip antenna," *IEEE Trans. Antennas Propag.*, vol. 67. no. 5, pp: 3461-3466, May 2019. doi: 10.1109/tap.2019.2902750.

[6] A. Khidre, K.-F. Lee, F. Yang, and A. Z. Elsherbeni, "Circular polarization reconfigurable wideband e-shaped patch antenna for wireless applications," *IEEE Trans. Antennas Propag.*, vol. 61. no. 2, pp: 960-964, Feb. 2013. doi: 10.1109/tap.2012.2223436.

[7] H. Aissat, L. Cirio, M. Grzeskowiak, J. M. Laheurte, and O. Picon, "Reconfigurable circularly polarized antenna for short-range communication systems," *IEEE Trans. Microw. Theory Techn.*, vol. 54. no. 6, pp: 2856-2863, June 2006. doi: 10.1109/tmtt.2006.875454.

[8] W. Lin, S.-L. Chen, R. W. Ziolkowski, and Y. J. Guo, "Reconfigurable, wideband, low-profile, circularly polarized antenna and array enabled by an artificial magnetic conductor ground," *IEEE Trans. Antennas Propag.*, vol. 66. no. 3, pp: 1564-1569, Mar. 2018. doi: 10.1109/tap.2018.2790437.

[9] H. H. Tran, N. Nguyen-Trong, T. T. Le, and H. C. Park, "Wideband and multipolarization reconfigurable crossed bowtie dipole antenna," *IEEE Trans. Antennas Propag.*, vol. 65. no. 12, pp: 6968-6975, Dec. 2017. doi: 10.1109/tap.2017.2766439.

[10] F. Wu and K. M. Luk, "Single-port reconfigurable magneto-electric dipole antenna with quad-polarization diversity," *IEEE Trans. Antennas Propag.*, vol. 65. no. 5, pp: 2289-2296, May 2017. doi: 10.1109/tap.2017.2681437.

[11] M. Ikram, N. Nguyen-Trong, and A. Abbosh, "A simple single-layered continuous frequency and polarization-reconfigurable patch antenna array," *IEEE Trans. Antennas Propag.*, pp: 4991-4996, June 2019. doi: 10.1109/tap.2019.2952461.

[12] Q. Pei-Yuan, Y. J. Guo, C. Yong, E. Dutkiewicz, and L. Chang-Hong, "A reconfigurable antenna with frequency and polarization agility," *IEEE Antennas Wireless Propag. Lett.*, vol. 10. pp: 1373-1376, 2011. doi: 10.1109/lawp.2011.2178226.

[13] J. Hu, et al., "A reconfigurable 1 × 4 circularly polarized patch array antenna with frequency, radiation pattern, and polarization agility," *IEEE Trans. Antennas Propag.*, vol. 69. no. 8, pp: 5124-5129, Aug. 2021. doi: 10.1109/tap.2020.3048526.

[14] J. M. Kovitz, H. Rajagopalan, and Y. Rahmat-Samii, "Design and implementation of broadband mems rhcp/lhcp reconfigurable arrays using rotated e-shaped patch elements," *IEEE Trans. Antennas Propag.*, vol. 63. no. 6, pp: 2497-2507, June 2015. doi: 10.1109/tap.2015.2417892.

[15] H.-J. Dong, Y.-B. Kim, and H. L. Lee, "Reconfigurable quad-polarization switched beamforming antenna with crossed inverted-v array and dual-butler matrix," *IEEE Trans. Antennas Propag.*, vol. 70. no. 4, pp: 2708-2716, Apr. 2022. doi: 10.1109/tap.2021.3137258.

[16] J. A. Ruiz-Cruz, M. M. Fahmi, S. A. Fouladi, and R. R. Mansour, "Waveguide antenna feeders with integrated reconfigurable dual circular polarization," *IEEE Trans. Microw. Theory Techn.*, vol. 59. no. 12, pp: 3365-3374, Dec. 2011. doi: 10.1109/tmtt.2011.2170581.

[17] A. Arbelaez, I. Goode, J. Gomez-Cruz, C. Escobedo, and C. E. Saavedra, "Liquid metal reconfigurable patch antenna for linear, rh, and lh circular

polarization with frequency tuning," *Can. J. Electr. Comput. Eng.*, vol. 43. no. 4, pp: 218-223, Fall 2020. doi: 10.1109/cjece.2019.2904898.

[18] C. Xu, Z. Wang, Y. Wang, P. Wang, and S. Gao, "A polarization-reconfigurable wideband high-gain antenna using liquid metal tuning," *IEEE Trans. Antennas Propag.*, vol. 68. no. 8, pp: 5835-5841, Aug. 2020. doi: 10.1109/tap.2020.2996773.

[19] P. Wang, Y. Jia, Y. Liu, and W. Hu, "A wideband low-rcs circularly polarized reconfigurable c-shaped antenna array based on liquid metal," *IEEE Trans. Antennas Propag.*, vol. 70. no. 9, pp: 8020-8029, Sept. 2022. doi: 10.1109/tap.2022.3164179.

[20] G. B. Zhang, et al., "A liquid-metal polarization-pattern-reconfigurable dipole antenna," *IEEE Antennas Wireless Propag. Lett.*, vol. 17. no. 1, pp: 50-53, Jan. 2018. doi: 10.1109/lawp.2017.2773076.

[21] L. Song, W. Gao, and Y. Rahmat-Samii, "3-d printed microfluidics channelizing liquid metal for multipolarization reconfigurable extended e-shaped patch antenna," *IEEE Trans. Antennas Propag.*, vol. 68. no. 10, pp: 6867-6878, Oct. 2020. doi: 10.1109/tap.2020.2993079.

[22] C. Wang, J. C. Yeo, H. Chu, C. T. Lim, and Y.-X. Guo, "Design of a reconfigurable patch antenna using the movement of liquid metal," *IEEE Antennas Wireless Propag. Lett.*, vol. 17. no. 6, pp: 974-977, June 2018. doi: 10.1109/lawp.2018.2827404.

[23] H. Xing, et al., "Three-polarization-reconfigurable antenna array implemented by liquid metal," *IEEE Antennas Wireless Propag. Lett.*, vol. 23. no. 1, pp: 374-378, Jan. 2024. doi: 10.1109/lawp.2023.3325217.

[24] Y. Liu, Q. Wang, Y. Jia, and P. Zhu, "A frequency- and polarization-reconfigurable slot antenna using liquid metal," *IEEE Trans. Antennas Propag.*, vol. 68. no. 11, pp: 7630-7635, Nov. 2020. doi: 10.1109/tap.2020.2993110.

[25] H. Liu, T. Yan, Z. Zhao, Z. Wang, and S. Fang, "Polarization-reconfigurable compact wideband slot antenna by using liquid metal," *IEEE Antennas Wireless Propag. Lett.*, vol. 21. no. 12, pp: 2327-2331, Dec. 2022. doi: 10.1109/lawp.2022.3192529.

[26] Y. Zhang, S. Lin, D. Qin, Q. Ding, and X. Zhang, "A wideband polarization reconfigurable orthogonal-dipole antenna controlled by liquid metal switches," *IEEE Antennas Wireless Propag. Lett.*, pp: 1-5, Dec. 2023. doi: 10.1109/lawp.2023.3301025.

[27] S. J. Mazlouman, J. Xing Jie, A. Mahanfar, C. Menon, and R. G. Vaughan, "A reconfigurable patch antenna using liquid metal embedded in a silicone substrate," *IEEE Trans. Antennas Propag.*, vol. 59. no. 12, pp: 4406-4412, Dec. 2011. doi: 10.1109/tap.2011.2165501.

[28] C. Shi, W. Zhigang, P. Hallbjorner, K. Hjort, and A. Rydberg, "Foldable and stretchable liquid metal planar inverted cone antenna," *IEEE Trans. Antennas Propag.*, vol. 57. no. 12, pp: 3765-3771, Dec. 2009. doi: 10.1109/tap.2009.2024560.

[29] Y.-W. Wu, S. Alkaraki, S.-Y. Tang, Y. Wang, and J. R. Kelly, "Circuits and antennas incorporating gallium-based liquid metal," *Proc. IEEE*, vol. 111. no. 8, pp: 955-977, Aug. 2023. doi: 10.1109/jproc.2023.3285400.

[30] X. Tan and Y. Zhang, "Tunable couplers: An overview of recently developed couplers with tunable functions," *IEEE Microwave Mag.*, vol. 24. no. 3, pp: 20-33, Mar. 2023. doi: 10.1109/mmm.2022.3226550.

[31] S. Zheng, W. Chan, and Y. Wong, "Reconfigurable rf quadrature patch hybrid coupler," *IEEE Trans. Ind. Electron.*, pp: 3349-3359, Aug. 2012. doi: 10.1109/tie.2012.2200224.

[32] D. M. Pozar, *Microwave engineering (4ed)*. 2012: Wiley.

[33] Y.-W. Wu, S.-Y. Tang, J. Churm, and Y. Wang, "Liquid metal-based tunable linear phase shifters with low insertion loss, high phase resolution, and low dispersion," *IEEE Trans. Microw. Theory Techn.*, vol. 71. no. 9, pp: 3968-3978, Sept. 2023. doi: 10.1109/tmtt.2023.3248954.

[34] Y.-W. Wu, L. Qian, J. Churm, and Y. Wang, "Liquid metal-enabled filtering switches and switchplexers," *IEEE Trans. Microw. Theory Techn.*, pp: 1-12, 2024. doi: 10.1109/tmtt.2024.3357968.

[35] Y.-Q. Wen, S. Gao, B.-Z. Wang, and Q. Luo, "Dual-polarized and wide-angle scanning microstrip phased array," *IEEE Trans. Antennas Propag.*, vol. 66. no. 7, pp: 3775-3780, July 2018. doi: 10.1109/tap.2018.2835521.

[36] L. L. Shafai, W. A. Chamma, M. Barakat, P. C. Strickland, and G. Séguin, "Dual-band dual-polarized perforated microstrip antennas for sar applications," *IEEE Trans. Antennas Propag.*, vol. 48. no. 1, pp: 58-66, Jan. 2000. doi: 10.1109/8.827386.

[37] T. Chaloun, V. Ziegler, and W. Menzel, "Design of a dual-polarized stacked patch antenna for wide-angle scanning reflectarrays," *IEEE Trans. Antennas Propag.*, vol. 64. no. 8, pp: 3380-3390, Aug. 2016. doi: 10.1109/tap.2016.2570804.

[38] L. Y. Yi, He; Dai, Manyuan; Wang, He; Yang Hu, "Design of a ka/ku dual-band dual-polarized array," *2014 3rd Asia-Pacific Conference on Antennas and Propagation*, 2014.

[39] T. H. Jang, H. Y. Kim, D. M. Kang, S. H. Kim, and C. S. Park, "60 ghz low-profile, wideband dual-polarized u-slot coupled patch antenna with high isolation," *IEEE Trans. Antennas Propag.*, vol. 67. no. 7, pp: 4453-4462, July 2019. doi: 10.1109/tap.2019.2911623.

[40] E. Gonzalez and G. Mumcu, "Integrated actuation of microfluidically reconfigurable mm-wave spst switches," *IEEE Microwave Wireless Compon. Lett.*, vol. 29. no. 8, pp: 541-544, Aug. 2019. doi: 10.1109/lmwc.2019.2925889.